Oscillator Finite-Difference Time-Domain (O-FDTD) electric field propagation model: integrated photonics and networks

Ricardo M. R. Adão[1], *Manuel* Caño-Garcia[1], *Christian* Maibohm[1], *Bruno* Romeira[1], and *Jana B.* Nieder[1,*]

[1]INL – International Iberian Nanotechnology Laboratory, Av. Mestre José Veiga s/n, 4715-330 Braga, Portugal

Abstract. The recently developed Lorentz Oscillator Model-inspired Oscillator Finite-Difference Time-Domain (O-FDTD) is one of the simplest FDTD models ever proposed, using a single field equation for electric field propagation. We demonstrate its versatility on various scales and benchmark its simulation performance against theory, conventional FDTD simulations, and experimental observations. The model's broad applicability is demonstrated for (but not limited to) three contrasting realms: integrated photonics components on the nano- and micrometer scale, city-wide propagating radiofrequency signals reaching into the hundreds of meters scale, and for the first time, in support of 3D optical waveguide design that may play a key role in neuromorphic photonic computational devices.

1 Introduction

Photonic simulation algorithms are crucial tools to understand, engineer, and optimize the optical properties of photonic structures in myriad applications. Discrete time-domain electrodynamic simulation models include Finite-Difference Time-Domain (FDTD), Finite-Element Time-Domain (FETD), Discontinuous Galerkin Time-Domain (DGTD), among others [1], most of them either solving or applying Maxwell's field equations over time. Still, novel system-specific or more efficient methods are developed continuously [2]. Here we use the new, simplified approach for dielectric and semiconductor materials, called Oscillator Finite-Difference Time-Domain (O-FDTD) [3]. The approach considers a mesh of coupled oscillators that allow electric field waves to propagate through space and matter. We aim to demonstrate its applicability versatility, ranging from planar photonic micro and nanostructures to RF signal coverage in cityscape environments [4].

Planar photonic devices embody countless applications ranging from biosensing [5] to photonic computing [6]. Most dielectric and semiconductor devices rely on coherent effects such as waveguiding, interference, and resonances. To showcase O-FDTD's applicability, we select a few of the most widely used photonic building blocks, such as Multimode Interferometers (MMI), photonic crystals, and microring resonators. We aim to simulate the device's performance and compare it against theoretical predictions and simulations using established FDTD software.

The interest in lightwave propagation simulations is not limited to the micro/nanoscale. With the raging demand of Smart Cities and the Internet of Things (IoT) comes the urgent need for efficient long-range wireless technologies such as Long Range (LoRa) [7], and the ability to accurately predict the signal strength and coverage towards effective network planning. We aim to push the boundaries of conventional photonic simulations and explore O-FDTD's applicability to complex, large-scale systems in the RF range by simulating a LoRa network coverage in a cityscape environment [4].

In the current fast-forward technological age, computation power and efficiency are vital, where photonic computation is the most promising fast and low-power alternative to conventional computing. In particular, photonic neuromorphic platforms promise hardware-based artificial intelligence implementations such as artificial neural networks [6]. Alongside the spiking neuron device, the on-chip interconnection of complex neuron architectures avoiding channel superposition and crosstalk remains challenging. At the same time, polymeric structures with unique properties and 3D fabrication processes arise as promising photonic elements [8], and recent works have reported on the use of 3D polymeric waveguides to interconnect photonic neural networks [9]. We aim to break O-FDTD's 2D limitation to study 3D polymeric waveguides towards micro-LED-based spiking neuron interconnections.

2 O-FDTD Theoretical model

O-FDTD addresses propagating electric field waves similarly to mechanical oscillations. Hendrik Lorentz first proposed using electron oscillations to quantify electric fields in the widely known Lorentz Oscillator Model (LOM) [10]. Instead of isolated, material-limiting electrons, one can consider a mesh of massless coupled oscillators. The oscillators move proportionally to the electric field amplitude, thus allowing waves to propagate as mechanical waves propagate over liquid surfaces (see water pond-like illustration in **Fig. 1**).

* Corresponding author: jana.nieder@inl.int

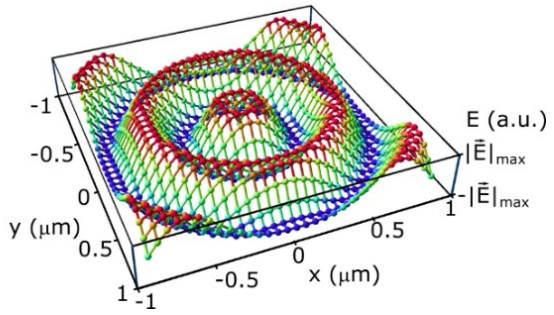

Fig. 1. O-FDTD electric field spatial distribution illustration. Each oscillator is coupled to its neighbors, allowing electric field wave propagation. (modified from [2]).

In O-FDTD, the electric field E temporal discretization is achieved via a simple leapfrog time backward differentiation

$$E_i = E_{i-1} + \frac{\mathrm{d}E_{i-1}}{\mathrm{d}t}\delta t + \frac{1}{2}\frac{\mathrm{d}E_{i-1}}{\mathrm{d}t}\delta t^2, \quad (1)$$

where $\mathrm{d}/\mathrm{d}t$ and δt are the time derivative and time-step, respectively, and E_i is the electric field amplitude in iteration i. From an analogy with the LOM, we express the wave equation of the coupled oscillators as:

$$\frac{\mathrm{d}^2E_{i-1}}{\mathrm{d}t^2} = \Gamma\left(E_{i-1}^{Neigh} - E_{i-1}\right) - \gamma\frac{\mathrm{d}E_{i-1}}{\mathrm{d}t}, \quad (2)$$

where $\gamma \propto 4\pi\kappa$ relates to the material absorption coefficient (imaginary part of the refractive index). The coupling strength Γ defines the electric field transfer rate between adjacent couplers and thus the speed of light in the medium,

$$\Gamma = \frac{8}{3n^2\delta t^2}, \quad (3)$$

where n is the real part of the material refractive index. E^{neigh} is the average neighborhood electric field, calculated by a unitary Ω kernel matrix (box blur) convolution of the electric field $E_{i\text{-}1}$. The final O-FDTD formulation can be expressed as

$$\frac{\mathrm{d}^2E_{i-1}}{\mathrm{d}t^2} = \frac{8(\Omega * E_{i-1} - E_{i-1})}{3n^2\delta t^2} - \frac{\sqrt{2}c}{n}\frac{4\pi\kappa}{\lambda}\frac{\mathrm{d}E_{i-1}}{\mathrm{d}t}, \quad (5)$$

Where c and λ are the vacuum speed of light and wavelength. A simple O-FDTD simulation algorithm can be implemented by defining a rectangular-meshed refractive index map, light sources, and boundary conditions. In this proof-of-concept, light sources are implemented by localized sinusoidal electric field inputs $E_i^{source} = E_i + E_0\sin(2\pi ct_i/\lambda)$, where E_0 and t_i are the input electric field amplitude and the time. Perfectly Matched Layer (PML) boundary conditions are implemented by surrounding the simulation space with artificial layers of linearly increasing absorption coefficient κ. Detailed implementation descriptions can be found in the Supplemental Document of ref [3].

3 Results

Here we demonstrate O-FDTD's broad applicability to photonic structures and wavelength ranges by showcasing examples from planar integrated circuit building blocks (**3.1**) to RF signals propagating in urban environments (**3.2**). We furthermore present a symmetry-based approximation to extend O-FDTD's 2D model to out-of-plane light extraction using 3D polymeric waveguides.

3.1 Planar dielectric photonics

Fig. 2 shows the electric field amplitude maps for three of the most relevant PIC building blocks. **Fig. 2(a)** shows a simple Si/SiO_2 core/cladding 1x4 rectangular MMI that splits an input signal into four equal outputs, with a 90% efficiency. **Fig. 2(b)** shows a 2D Si/air pillar array-based photonic crystal with a pillar radius r = 100 nm, lattice constant a = 635.5 nm, wavelength λ = 1.55 μm, and angle θ = 60°. The photonic bandgap was calculated using MIT Photonic-Bands [11]. A "z-shaped" photonic crystal waveguide (gap) induces two 120° sharp bends, unsupported by "conventional" waveguides. **Fig. 2(c)** shows a 3 μm radius Si/SiO_2 core/cladding microring resonator driven at 1945 and 1970 nm. The two wavelengths excite off and on-resonance states, where the light is outputted via the *Through* (top) and *Drop* (bottom) waveguides, respectively.

Other O-FDTD applications to photonic microstructures can be found in ref [3], where the results are validated against theory, conventional FDTD simulations, and experimental observations. Having demonstrated O-FDTD's applicability to micro and nanostructures in the visible and infrared wavelength regimes, many other electromagnetic simulation applications are conceivable, as explored in the following section.

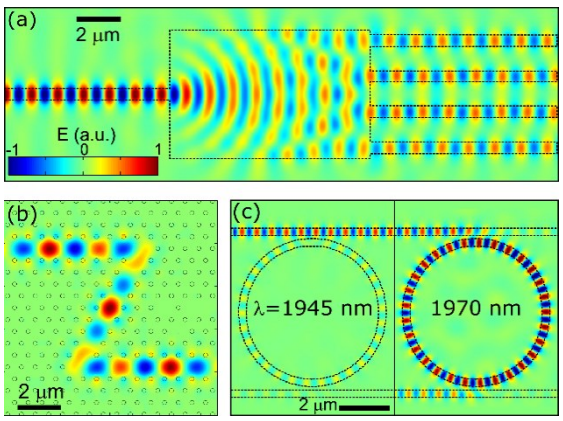

Fig. 2 Planar semiconductor (Si-air) photonic components. (a) Multi-Mode Interferometer. (b) Photonic-crystal waveguide. (c) Photonic ring resonator (modified from [2]).

3.2 Cityscape LoRa network coverage

RF antennas in urban environments (both indoors and outdoors) can be seen as dipole electric field sources surrounded by different dielectric constant materials in complex arrangements. **Fig. 3(a)** shows the O-FDTD-simulated electric field power (Receiver Signal Strength Indicator (RSSI)) propagating in a city-wide environment [4]. The simulation models concrete walls via their dielectric constant and real-world building data from Google Maps. The binary (on-off) coverage area map is obtained by considering a -124 dBm receiver sensitivity threshold and is compared against the experimental characterization in **Fig. 3(b)**. The red, green, and yellow channels represent the isolated simulated, experimental, and overlapping areas. The simulation-experiment agreement can be expressed by coverage area overlap, **Fig. 3(b-c),** or edge variation, **Fig. 3(d)**. We obtain a considerable area overlap of 84%. However, this measure underestimates the rich O-FDTD-predicted reflection and interference pattern since all coverage models predict good coverage near the emitter. Most path loss-based coverage models only provide an average coverage distance and thus a circular coverage area. **Fig. 3(d)** compares the angle-dependent coverage (emitter-to-edge) distance experimental-simulation difference obtained with O-FDTD and the best-fitting circle. We obtain root mean square (RMS) errors of 24 and 41 m, respectively. Considering that the best-fitting circle (error minimizer) is an experiment-biased result, it is reasonable to assume that unbiased predictions will only yield larger errors. These results indicate that such simplistic path-loss models would yield at least twice the average O-FDTD coverage edge error.

Despite O-FDTD's 2D formulation, the following section describes how symmetry assumptions extend the model to some 3D architectures.

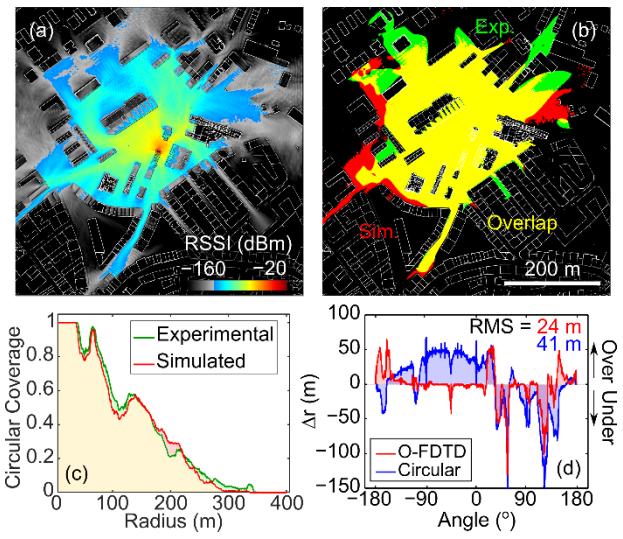

Fig. 3. Cityscape LoRa Propagation. (a) Simulated RSSI map. (b) Simulation versus experimental coverage areas. Quantitative area (c) and (d) edge comparison (modified from [3]).

3.3 3D interconnects for neural networks

The proposed interconnected photonic neural network concept is illustrated in **Fig. 4(a)**. Semiconductor (GaAs / AlGaAs) epilayer stacks aim to provide light sources with neuron-mimicking spiking properties interconnected into artificial neural networks by 3D polymeric waveguides. As a starting point, we consider 4 μm wide micropillar LEDs using SiO_2 as a passivation layer and Au as an electrical contact.

Assuming that a 3D waveguide extends over a single plane, we can estimate its waveguiding properties by simulating the electric field propagation along its longitudinal section. **Fig. 4(b)** shows the O-FDTD E^2 simulation of the micro-LED light emission without **(b1)** and with **(b2)** a 3D polymeric (OrmoCore, n = 1.56) outcoupling waveguide. **Fig. 4(b1)** reveals two main emission directions or components of similar intensity: a vertical component that escapes towards air and a horizontal component trapped within the SiO_2 layer. Simple polymeric structures can be designed for vertical or horizontal outcoupling. For ease of fabrication, we choose the horizontal. **Fig. 4(b2)** shows the efficient extraction of the horizontal component otherwise trapped in the SiO_2 layer. **Fig. 4(c)** shows the propagation across an entire waveguide structure, where some support structure-induced scattering can be observed.

Discussion

O-FDTD is an unprecedented simple, single-equation electrodynamic model that can readily implement photonic simulation algorithms. Empirical simulations demonstrate that the complex refractive index-dependent field modulation accurately reproduces bulk and interface light-matter interactions in some of the most widely used photonic device components. However, O-FDTD's simplicity comes at the cost of a few limitations. Firstly, the present formulation assumes orthogonality between the electric field oscillation and the propagation plane, thus limiting it to TM polarization.

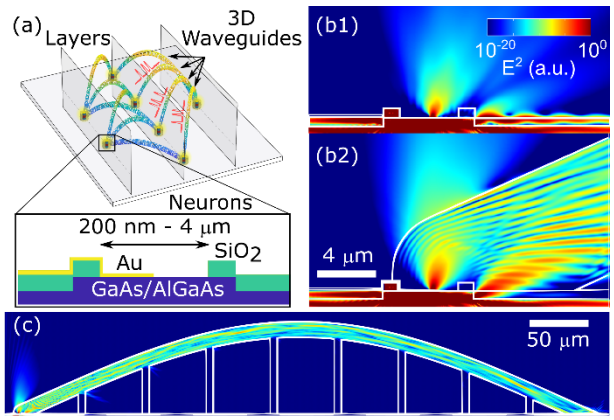

Fig. 4. 3D waveguides for photonic neuromorphic computing. (a) 3D-interconnected planar neural network concept. (b) Light outcoupling from GaAs/AlGaAs micro-LED at λ = 850 nm. (c) Light propagation in a supported waveguide.

Secondly, this orthogonality requirement limits O-FDTD to 2D simulations, as extrapolating it to 3D would lead to unrealistic (soundwave-like) propagation-direction electric field oscillations. Thirdly, the present O-FDTD formulation disregards the electric conductivity, making it less than optimal for metals. Furthermore, Eq. (5) shows that $n < 1$ materials (e.g., metals in the UV) can lead to enlarged coupling strengths and algorithm divergence. Higher mesh densities (resolution) help reduce the divergence at the cost of longer simulation times. Notwithstanding, the simulation results presented in this work demonstrate its vast wavelength range and system applicability.

The core/cladding refractive index contrast in Si/SiO_2 devices leads to single and multi-mode waveguiding and interference patterns matching the typical self-imaging symmetric MMI interference predicted theoretically. Cavity geometry optimization and input/output tapering can minimize the splitting losses but are beyond the scope and intent of this work. The photonic crystal waveguiding in **Fig. 2(b)** demonstrates the photonic crystal bandgap concept in periodic subwavelength structures. The add-drop microring simulations demonstrate resonant interference effects.

However, O-FDTD's potential is not restricted to the micro/nanoscale. Since the laws of electromagnetism hold for any wavelength range, we put O-FDTD's applicability to the test in a 360000 m^2 cityscape environment. **Fig. 3(d)** compares O-FDTD against the best-fitting path loss model. However, these are the simplest and most limited models. More sophisticated real-world data-based coverage prediction algorithms such as ray-tracing [12] and diffraction-based [13] models take map-specific effects into account, such as reflections, scattering, and diffraction. Other models, such as the Irregular Terrain Model (ITM), consider terrain elevation and climacteric conditions. Each approach has pros and cons and optimal application conditions. To name a few challenges: The quality of ray-based models is usually statistics or ray-density dependent; diffraction models are usually limited to simplified geometries; ITM is best suited for large-scale networks but provides low inter-building resolution; wave propagation-based models are forbiddingly computationally demanding for city-wide areas. On the other hand, the single-equation O-FDTD approach holds the promise for next-generation wave-propagation methods for indoor and outdoor high-precision network coverage predictions. This work opens broad perspectives for high-precision electromagnetic signal distribution predictions in wireless networks, particularly in modern Smart City and Internet IoT technologies.

Lastly, we report a sectioning approximation to extend O-FDTD's applicability to specific 3D problems. It is worth mentioning that this method does not allow the complete simulation of the 3D system. Notwithstanding, in this example, it provides vital information on the microLED emission angle and extraction achievable with standing polymeric waveguides. Significantly, it is observed that a fraction (~50%) of otherwise lost emission to the passivation layer can be collected. Strategies for off-vertical axis light extraction from the biomimicking neurons can be obtained by simulation-powered 3D waveguide optimization, including parameters such as core dimensions, outcoupling angle, bending radii, and support structures. The dimensions and number of support structures depend strongly on the mechanical stability of the TPP polymer and need to be optimized using mechanical models or experimental trials.

Conclusion

Our recently developed O-FDTD method [3] can model electric field wave propagation in different media by modeling matter as a mesh of oscillators coupled with a complex refractive index-dependent coupling strength. The O-FDTD model's accuracy is validated against theory, simulation, and experimental observations in various contexts, in and beyond photonics. Despite its polarization, dimensionality, and material limitations, we demonstrate its applicability to a vast set of commonly used photonic building blocks, both 2D and 3D. The model holds tremendous potential for dielectric and semiconductor photonics, PICs, and other wave propagation technologies, from UV to RF.

This work was funded by the European Commission (H2020-FET-OPEN No. 828841 "ChipAI") and ERDF (0181_NANOEATERS_1_EP). RA acknowledges the Laser Photonics & Vision Ph.D. program, U. Vigo.

References

1. U. S. Inan and R. A. Marshal, *Numerical Electromagnetics*, 1st ed. (Cambridge University Press, 2011).
2. Q. Sun, R. Zhang, Q. Zhan, and Q. H. Liu, IEEE Trans. Antennas Propag. **67**(8), 5469–5476 (2019).
3. R. M. R. Adão, M. Caño-García, C. Maibohm, and J. B. Nieder, Opt. Express **29**(8), 11903–11916 (2021).
4. R. M. R. Adão, E. Balvís, A. V Carpentier, H. Michinel, and J. B. Nieder, Sensors **21**(8), 2717 (2021).
5. W. Bogaerts, P. de Heyn, T. van Vaerenbergh, K. de Vos, S. Kumar Selvaraja, T. Claes, P. Dumon, P. Bienstman, D. van Thourhout, and R. Baets, Laser Photonics Rev. **6**(1), 47–73 (2012).
6. B. Romeira, J. M. L. Figueiredo, and J. Javaloyes, Nanophotonics **9**(13), 4149–4162 (2020).
7. U. Raza, P. Kulkarni, and M. Sooriyabandara, IEEE Communications Surveys & Tutorials **19**(2), 855–873 (2017).
8. M. C. Oh, W. S. Chu, J. S. Shin, J. W. Kim, K. J. Kim, J. K. Seo, H. K. Lee, Y. O. Noh, and H. J. Lee, Opt. Commun. **362**, 3–12 (2016).
9. J. Moughames, X. Porte, M. Thiel, G. Ulliac, L. Larger, M. Jacquot, M. Kadic, and D. Brunner, Optica **7**(6), 640-646 (2020).
10. A. F. J. Levi, "The Lorentz oscillator model," in *Essential Classical Mechanics for Device Physics*, 1st ed. (Morgan and Claypoll Publishers, 2016), p. 101.
11. S. G. Johnson and J. D. Joannopoulos, (2015).
12. F. Firdaus, N. A. Ahmad, and S. Sahibuddin, Sensors (Switzerland) **19**(24), 5546 (2019).
13. S. A. Vavilov and M. S. Lytaev, IEEE Trans. Antennas Propag. **68**(5), 3859–3877 (2020).